Behaviour of post-installed adhesive anchors in natural stone

Article *in* Construction and Building Materials · October 2014

DOI: 10.1016/j.conbuildmat.2014.05.099

2 authors:

Loredana Contrafatto
University of Catania
59 PUBLICATIONS **242** CITATIONS
SEE PROFILE

Renato Cosenza
University of Catania
2 PUBLICATIONS **5** CITATIONS
SEE PROFILE

Construction and Building Materials 68 (2014) 355–369

Contents lists available at ScienceDirect

Construction and Building Materials

journal homepage: www.elsevier.com/locate/conbuildmat

Behaviour of post-installed adhesive anchors in natural stone

Loredana Contrafatto [a,*], Renato Cosenza [b]

[a] Department of Civil and Environmental Engineering, University of Catania, Italy
[b] Laboratory of Structural and Material Testing, University of Catania, Italy

HIGHLIGHTS

- Experimental research on chemical anchors in natural stone.
- Embedment length of chemically post-installed threaded rods in basalt, sandstone and limestone support.
- Evaluation of the reliability of theoretical formulations in the literature valid for concrete.
- Investigation on the applicability of numerical models for the prediction of the bearing capacity of the anchor.
- High impact of the paper on the knowledge about adhesive anchors in natural stone given the lack of data on the topic.

ARTICLE INFO

Article history:
Received 16 January 2014
Received in revised form 28 May 2014
Accepted 30 May 2014

Keywords:
Adhesive anchors
Epoxy resin
Threaded rods
Sandstone
Basalt
Limestone
Fracture

ABSTRACT

This work is based on the results of an experimental research related to chemical anchors in natural stone. The specific goal is to achieve the minimum embedment depth for chemical anchoring of post-installed threaded rods in basalt, sandstone and limestone support, by using epoxy resin. The reliability of theoretical formulations in the literature valid for concrete is evaluated. The applicability of some numerical models for the prediction of the bearing capacity of the anchor is then investigated, whereas the theoretical formulations are not feasible.

1. Introduction

In most countries of the world, the building stock is ageing and needs continuous maintenance or repair. Moreover, the majority of existing constructions is deficient in the light of current knowledge and design codes. The problem of the structural deficiency of existing constructions is especially acute in seismic regions, as, even there, seismic design of structures is relatively recent. The direct and indirect costs of demolition and reconstruction of structurally deficient constructions are often prohibitive; furthermore they entail a substantial waste of natural resources and energy. Therefore, structural retrofitting is becoming increasingly widespread throughout the world.

Additional consideration can be made concerning masonry. Masonry was, in the past, and is, today, one of the most commonly used materials throughout the world for the construction of low rise buildings.

Even though the history of past earthquakes has shown that masonry buildings suffered the high damage and accounted for the loss of life, they constitute almost the entirety of the historic centre constructions. The stonework is largely widespread in different countries and despite the variety of materials and techniques used, it has recurring problems regarding both the vulnerability to seismic actions and the applicability of reinforcement techniques.

There are many types of remedial measures that can be implemented on masonry buildings in order to improve their dynamic characteristics. In particular, in the context of the retrofitting of existing buildings, a great development has been achieved with the use of anchoring systems, understood as real structural elements.

The anchoring systems, in particular those with chemical anchors, are commonly used in plain or reinforced concrete

* Corresponding author.
E-mail addresses: loredana.contrafatto@dica.unict.it (L. Contrafatto), renato.cosenza@studium.unict.it (R. Cosenza).

http://dx.doi.org/10.1016/j.conbuildmat.2014.05.099
0950-0618/

structures but also in structures in lightweight material, such as wood and brick, and in masonry constructions to rigidly couple different structural elements. A variety of metal elements are usually involved in the anchoring system, normally steel elements (stirrups, longitudinal or shear reinforcement bars, threaded rods). The adhesive component of the system is generally resin, that usually found application in the structural strengthening and retrofitting of existing elements and in the addition or connection of new structural elements to other already existing.

Three types of resins for building are the most widespread on the market:

- vinyl with polyester, for anchoring of medium grip on walls in concrete, stone, bricks and hollow bricks, ideal for use in enclosed spaces because of their low toxicity;
- polyester with or without styrene, for specific, especially on masonry, anchors drilled through the use of the special cage (“sock”) that prevents the propagation through the voids of the masonry itself;
- epoxy, especially for hard anchorage on concrete elements, which generally are given as two part epoxy adhesive, chemical and heat resistance, good-to-excellent mechanical properties.

Nevertheless the specific legislation on the architectural heritage does not allow the use of resin on historical and monumental buildings, but suggest the usage of special mortars, there is a wide range of situations in which the use of chemical anchoring is more suitable than mortar, especially in the case of anchoring systems on rocks or high resistance supports. Such is the case of all the masonry buildings that are not under a preservation order or listed buildings.

However, for the last twenty years, such retrofitting techniques for masonry structures have been developed and practiced, but rarely validated with experiments and numerical modelling. Specifically, while a number of studies, both theoretical and experimental, concerns the behaviour of concrete anchors, the lack of data concerning the behaviour of chemical anchors in natural stone is incontrovertible.

A wide literature exists on the experimental behaviour of concrete anchors in terms of pull-out strength and anchor depth determination, as reported in [1–3].

The structural soundness of concrete reinforced with chemically bonded anchors have been studied by means of the use of acoustic emission techniques in [4]. A number of experimental investigations concerning concrete are also coupled with theoretical formulations for predicting the ultimate tension load [5–8], or the strength under shear load [9]. Moreover, experimental and theoretical predictions have been compared with numerical simulation by using elastoplastic finite-element analysis in [10], the 3D Microplane Concrete Model in [11] in the case of anchor bolts with large embedment depths, an elastic analysis in [12]. A detailed definition and characterisation of suitable adhesive material models for finite element analysis is given in [13]. Theoretical models for concrete have also been validated by Cook in [10], analytical and numerical support for the practical prediction of the strength of epoxy-grouted anchor bolts in reinforced concrete is provided in [14], while the pull-out behaviour of an imperfectly bonded anchor system is studied in [15]. The prediction of the tensile capacity of single adhesive using neural networks is attempted in [16]. Moreover, the extension of these concepts to Fiber Reinforced Polymer anchor can be found in [17,18], among others. In [19] the factors affecting the pull-out strength of steel rods bonded into precast concrete panels are investigated. The tensile behaviour of post-installed chemical anchors embedded to low strength concrete is studied in [20] and their response under cyclic load is analysed in [21]. Finally, the bond strength of chemical anchor in high-strength concrete is investigated from the experimental and numerical point of view in [22].

The literature drastically shrinks about other materials, such as wood. Cimadevila and co-authors presented a novel anchoring system using threaded steel rods glued into wood [23,24]. In the same way few paper are available, in the author knowledge, concerning stone materials. Some information can be found in [25] about the mechanical behaviour of anchorages for reinforcing marine stone structures subjected to sea waves, while the experimental investigation on mechanical and chemical anchors in masonry wall subject to pullout load and torque is reported in [26]. A few other references can be found in the field of rock mechanics and tunnelling technologies. In [27] the influence of the grout properties on the pull-out load capacity of fully cement-grouted rock bolts is investigated.

The poor information regarding the behaviour of chemical anchors in natural stone has highlighted the need of wide and deep researches in this area, especially required by licensed engineers working in the field.

Aim of the research is the determination of the uni-axial strength of post-installed threaded rods in natural stone by means of Hilti Re-500 epoxy resin of the company Hilti, providing technical guidelines for the determination of the minimum anchorage length in the case of block masonry.

The goal is achieved from both the experimental point of view (through laboratory testing) and the numerical point of view (through simulations with finite element software). In the experiments three different types of stone for construction were tested, at various embedment depth and for different values of the bar diameter. The validity of theoretical models for concrete is investigated.

The following is a brief description of the organisation of the paper.

Section 2 provides a general overview about chemical anchoring systems. In Section 3 there is a description of the materials that were used for both experimental and numerical studies concerning post-installed adhesive anchors in natural stone. Section 4 reports the results of the experimental investigations on chemically bonded anchoring systems in different stone types. Section 5 provides an overview of the theoretical models for the failure mechanisms of chemical anchors in the literature and section 5.2 the comparison between the theoretical prediction and the experimental results. In Section 6 the numerical simulation of the experimental tests in Section 4 is described and compared with test data. In Section 7 a specific algorithm based on the Strong Discontinuity Approach for the prediction of the cracks in brittle material is applied as an explanatory example of the failure mechanism. Some conclusions close the paper.

2. The anchoring system

In the past, traditional systems of fastening devices consisted of mortar to be applied after practising an hole of appropriate size on the wall.

Such systems are now almost entirely abandoned in favour of a widely used new generation of anchors. These modern fastening systems that use mechanical or chemical anchors, such as plastic or metal dowels, adhesive capsule or injectable resin mortar, require preliminary procedures, from the realisation of a single hole in the support by means of impact drill to the compressed-air cleaning of the hole.

The range of applications extends the anchors for attaching organs of various types to reinforced concrete, plain concrete, very compact stone walls, solid brick walls, semi-solid and perforated walls or heavy concrete blocks.

The anchors can be divided according to the type and/or the operating principle. Chemical type anchors work by adherence. Indeed, in this case, the resin effectively penetrates into the pores of the base material and into discontinuities, adhere to the roughness of the hole walls and, after curing and ageing, the transmission of the load to the support takes place by adhesion, the adhesion force being distributed along the entire anchor surface. The curing time mainly depends on two different factors: the type of formulation employed and the temperature of the environment in which the laying occurs.

The anchor agent is generally constituted by a two-part chemical adhesive, which allow to lock the anchoring bar inside the hole drilled in the holder. These anchors are suitable for heavy steel elements such as structural connections with post-installed rebars, structural or secondary steel connections (steel columns, beams, balustrades, ledgers). Depending on the implementation, they are distinguished in injection and vial systems.

Anchors injection cartridges are packed in hard or soft that contain the base resin and the hardener which, at the time of implementation, are mixed automatically in fixed proportions. The application is done using a special mixing nozzle or with a dispenser for silicone resins. The compound is applied within the hole and there blocks the gusset.

The post-installed chemical anchoring system is not explicitly set by the Italian legislation (Norme Tecniche per le Costruzioni 2008). According to the code, the resins used in the anchor, after the acquisition of a national Certificate of Technical Suitability or, alternatively, the European Techical Approval (ETA), can obtain the CE marking. The ETA is issued by a competent body according to the following Guidelines:

- ETA Guidelines (ETAG) 001 (1997 and amendment 2001, 2006, 2010): "Metal anchors for use in concrete". In Appendix C also the methods for the design of anchorages are given.
- Technical Report (TR 029, 2010): "Design of bonded anchors", which provides specific rules for this type of anchors.

This reference is the only internationally recognised today, but provides for a limited number of applications. The method proposed in the TR 029, is based on the evaluation of the resistance according to three mechanisms of rupture, and in particular:

1. if the depth of anchor is small, usually a breaking of concrete cone occurs;
2. if the depth of anchor is greater, a combined breakup develops, constituted by a surface concrete cone and a sliding below the cone;
3. if the depth of anchor is high, the anchor is so resistant that the break occurs in the steel bar.

The minimum depth to achieve the rupture of the bar represents the anchorage length, which depends on the quality of the steel and the properties of the resin and the stone.

For this reason, several manufacturers of resin have been inspired by the guidelines stated above to refine their methods of calculation, which would allow the design of anchorages in any form or characteristics. Some references can also be found in the UNI EN 1504-6.

For the anchors that involve the use of mortars, there is no single standard reference, but several provisions affecting the different behaviour of the mortar. For instance:

- bleeding – UNI 8998,
- expansion in the plastic phase – UNI 8996,
- restrained expansion – UNI 8147,
- adhesion to concrete cutting – UNI EN 12615,
- pull-out strength of steel bars – RILEM-CEB-FIP RC6-78,
- depth penetration of water – ISO EN 7031-94,
- elastic modulus – UNI 6556,
- compressive strength – UNI EN 196/1,
- tensile strength in bending – UNI EN 196/1.

Therefore, the present work was motivated by the absence of normative references regarding certain chemical anchors in natural stone and because of the fact that the investigations existing in the literature are scarce to get a complete picture of data.

An experimental campaign was developed to understand the behaviour of the aforementioned systems when the anchor support is constituted by natural stone. The minimum anchorage depth for threaded rods was determined. Three different rocks were considered in the tests, characterised by a significant difference in their mechanical properties, with the intent of representing some class of materials in the wide variety of rocks present in nature. In the following section the characterisation of the material realising the anchor is described.

3. Materials

Three types of natural stone, coming from local quarries, were used, typical of eastern Sicily: a sandstone from the southeast Sicily (Palagonia sandstone), a basalt stone from volcano Etna (Etna basalt) and a limestone from the region of the mountain chain of Nebrodi (Floresta limestone) (see Fig. 1(a–c)). Threaded steel rods were considered with three different nominal diameters. Hilti Re-500 epoxy resin by Hilti Corporation, Liechtenstein, was used.

3.1. Natural stones

The sandstone blocks that were used for the experiments were squared and all of size $15 \times 25 \times 45$ [cm^3]. The basalt blocks had quite irregular shape and dimensions ranging between $20 \times 20 \times 40$ [cm^3] to $30 \times 40 \times 60$ [cm^3]. The limestone blocks had also quite irregular shape and dimensions ranging between $20 \times 30 \times 40$ [cm^3] to $40 \times 40 \times 60$ [cm^3].

Uniaxial compression test were performed to characterise the compressive strength and the Young modulus of the rocks. The density of the materials was also evaluated. All the experimental tests took place at the Laboratory of Structural and Material Testing of Catania University.

The cubic specimens used for the uniaxial compression tests had dimensions $7 \times 7 \times 7$ [cm^3] (Fig. 2(a)). The prismatic specimens used to determinate the Young modulus had a square base of side 7 [cm] and height of 14 [cm] (Fig. 2(b)).

The base of the specimens was adjusted with a putty for marbles to ensure that the load was distributed over the entire base.

In Table 1 the mean value of the mechanical properties experimentally obtained is reported. Three samples for each type of rock were tested.

The uniaxial tensile strength was assumed equal to $\sigma_t = 50$ [N/mm^2] for basalt, $\sigma_t = 15$ [N/mm^2] for limestone and $\sigma_t = 1.5$ [N/mm^2] for sandstone.

3.2. Steel bars

Threaded metal rods are used in different engineering fields, such as civil or industrial construction industry. The threaded bars used in the experiments were unmarked, 4.6 class (tensile strength 400 [N/mm^2] and yield strength 240 [N/mm^2]). Three nominal diameters ϕ were considered: 10 [mm], 14 [mm], 20 [mm].

The uniaxial tensile test was performed to verify the tensile strength of the bars certified by the producer (Fig. 3). Table 2 reports the mean value of the strength for each diameter.

3.3. Epoxy resin

Epoxy resins are characterised by a greater mechanical strength and better adhesion to the drilled holes, than polyester or vinyl ester resins. The hardening time is approximately ten times greater. For these characteristics, they are mainly used for fastening of rods to various supports, also thanks to the greater fluidity which best suits injection in deeper holes.

The Hilti RE-500 epoxy resin was used. This system is a high strength, two part epoxy adhesive composed by: Component A (Epoxy resin, filler material) and Component B (hardener amine base, filler material). It consists of a side-by-side adhesive refill pack, a mixing nozzle, a HIT dispenser with refill pack holder. Hit-RE 500 is specifically designed for fastening into solid base materials such as concrete, grout, stone or solid masonry. HIT-RE 500 is also suitable for use under exceptional such as: underwater fastenings, oversized holes and diamond cored holes.

Fig. 1. (a) Palagonia sandstone samples. (b) Etna basalt samples. (c) Floresta limestone samples.

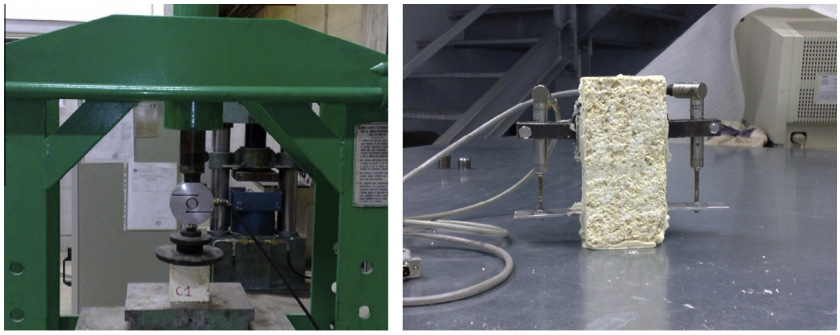

Fig. 2. Stone specimens for mechanical characterisation tests.

Table 1
Mechanical properties of the rocks.

Properties	Basalt	Limestone	Sandstone
σ_c [N/mm^2]	500	220	20
E [N/mm^2]	50,000	19,616	12,309
γ [kN/m^3]	30.0	26.0	14.3

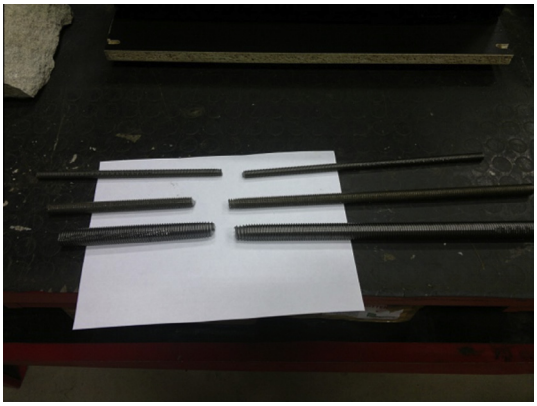

Fig. 3. Threaded rods after the tensile tests.

Table 2
Properties of threaded rods.

Diameter [mm]	Strength [MPa]	Force [kN]
$\phi = 10$	430.18	33.79
$\phi = 14$	431.30	66.39
$\phi = 20$	446.35	140.38

Table 3
Work and hardening time of Hilti RE-500 epoxy resin.

Temperature [°C]	Work times [min]	Curing time [h]
40	12	4
30–39	12	8
20–29	20	12
15–19	30	24
10–14	90	48
5–9	120	72

Table 4
Material properties of Hilti RE-500 epoxy resin.

Bond strength ASTM C882-91	
2 day cure	12.4 [MPa]
7 day cure	12.4 [MPa]
Compressive strength ASTM D-695-96	82.7 [MPa]
Compressive modulus ASTM D-695-96	1493 [MPa]
Tensile strength 7 day ASTM D-638-97	43.5 [MPa]
Elongation at break ASTM D-638-97	2.0%
Heat deflection temperature ASTM D-648-95	63 [C]
Absorption ASTM D-590-95	0.06%
Linear coefficient of shrinkage on cure ASTM D-2566-86	0.004
Electrical resistance DIN IEC 93 (12.93)	6.6×10^{13}

The manufacturer specifies the work and hardening times, given in Table 3 and the material properties given in Table 4:

4. Experimental tests

An experimental program was undertaken at the Laboratory of Structural and Material Testing of Catania University to investigate

the effects of the embedment length on the pull-out strength of the chemically bonded anchor system presented in Section 2.

According to Section 3, in the experimental planning the following parameters were taken into account: three kinds of rock (sandstone, basalt, limestone); three threaded rod nominal diameter (10 [mm], 14 [mm], 20 [mm]); three embedment depths (3, 5 and 10 times the bar diameter).

4.1. Testing instruments

The experimental tests consisted of applying a static pull-out force to the bar chemically bonded in the stone specimen. The test apparatus, shown in Fig. 4, was composed by: hydraulic cylinder (hollow cylinder of FPT CRM-30/100-FO Maximum pressure 700 bar); centesimal comparator (stroke length 50 [mm]); hand oleodynamic pump with connection pipes 2.5 [m]; HBM MGC Plus data acquisition system; triangular reaction frame with height-adjustable feet bearing on the stone block.

Because of the fact that many stone blocks had irregular faces, a welded triangular support with height-adjustable feet was used as a base for the hollow cylinder. The device had also the role of maintaining the zone possibly interested by crisis mechanism free from confinement.

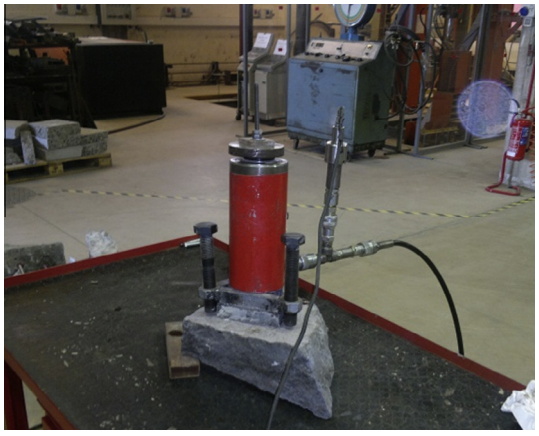

Fig. 4. Instrumentation for testing.

4.2. Installation

The installation of the anchorages was characterised by the following phases:

- **Drilling of the sample**: the drilling of each sample was performed by column drill. The diameter of the hole was always 4 [mm] larger than the rods diameter, considering an efficient thickness of resin of 2 [mm] all around the rod, as usually recommended in this applications.
- **Hole cleaning**: this is a very important stage because of the fact that the presence of dust inside the hole and on its wall surface prevents the optimal adhesion between the resin and the stone material; hole cleaning was carried out using compressed air and specific brushes.
- **Grouting the bars**: epoxy resin was injected into the hole and immediately the rod was inserted into the hole by screwing. The injection of the epoxy resin, contained in a side-by-side adhesive refill pack, was carried out by means of the HIT dispenser with refill pack holder. The amount of epoxy resin to be injected in each hole reached about 50–75% of the embedment depth.

4.3. Results of the experimental tests

Eighty-one tests were performed. Each test was labelled by using a 4-fields alphanumeric code. The first three field identify the series. For instance:

A	–	**10**	–	**3**	–	**1**
(1)		(2)		(3)		(4)

The alphabetic field identifies the stone type on which the experiment was done. A: Palagonia sandstone. B: Etna basalt. C: Floresta limestone. The first numeric field identifies the diameter of the bar. The second numeric field identifies the embedment depth L of the bar. The last numeric field identifies the number of the sample for each series. Typically the total number of samples in each series is 3. The code in the example indicates the test number 1 of the series, performed on sandstone block (A) with bar of diameter $\phi = 10$ [mm] and length of anchor $L = 3 \cdot \phi$ [mm].

When a rupture mechanism was characterised by the presence of a cone, the friction angle φ was measured as the geometric angle

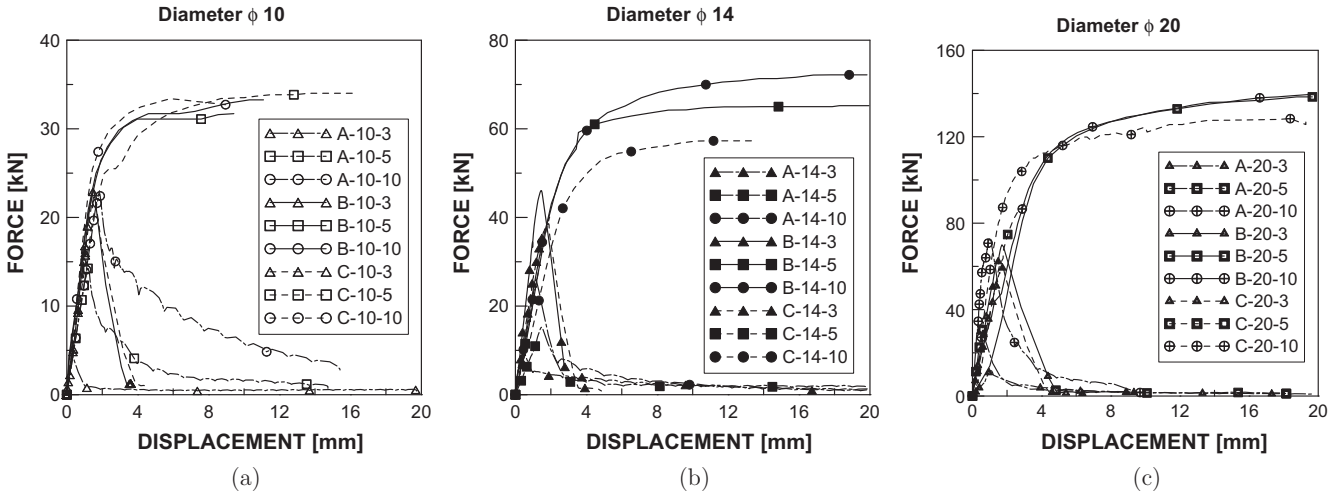

Fig. 5. Pull-out force–displacement diagram for different bar diameters. Influence of the embedment depth and of the material. (a) $\phi = 10$ [mm]. (b) $\phi = 14$ [mm]. (c) $\phi = 20$ [mm].

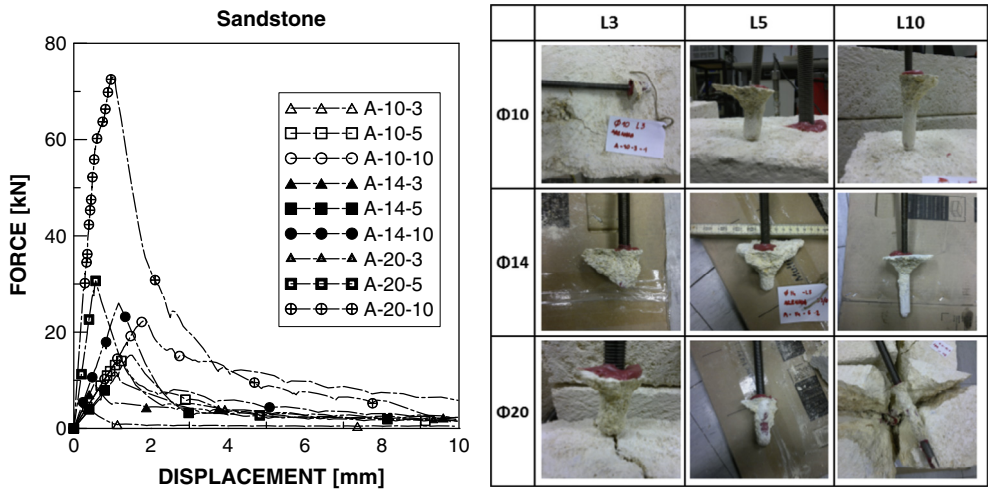

Fig. 6. Sandstone pull-out force–displacement diagram and failure mechanisms.

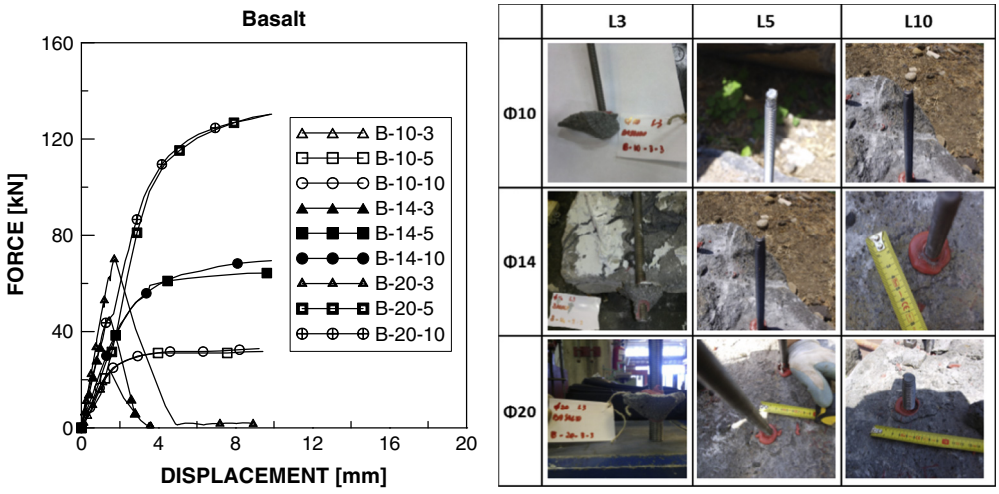

Fig. 7. Basalt pull-out force–displacement diagram and failure mechanisms.

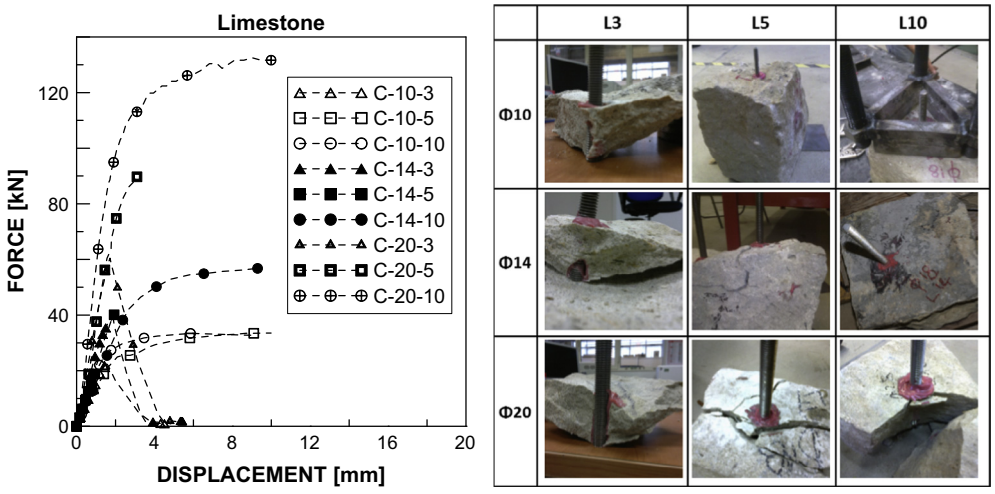

Fig. 8. Limestone pull-out force–displacement diagram and failure mechanisms.

between the sliding surface and the external top face of the sample.

Fig. 5(a–c) report the experimental curves for the three diameters $\phi = 10$ [mm], $\phi = 14$ [mm], $\phi = 20$ [mm] respectively.

Figs. 6(a), 7(a) and 8(a) show the comparison of the pull-out force for the different types of studied stones by varying the total embedment depth and for different values of the bar diameter. Figs. 6(b), 7(b), and 8(b) show the main failure mechanisms for each series.

In the case of basalt and limestone the failure mechanism was always characterised by the yielding of the bar for an embedment length equal to five or ten times the diameter (see Figs. 7(b) and 8(b)). Only for the length of anchor $L = 3 \cdot \phi$ the breaking process exhibited the formation of a stone cone.

On the contrary, in the case of sandstone, for each diameter and anchor length the failure was accompanied by the formation of a stone cone, eventually coupled with sliding at the rock/resin interface (see Fig. 6(b)).

When the sliding occurred, the real anchor length was consequently approximated to the height of the rupture cone. The resin detachment at the interface resin-rock was never observed, proving the excellent adhesive quality of the used resin.

Therefore, the minimum embedment length in the case of basalt and limestone is identified in the range $3 \cdot \phi \div 5 \cdot \phi$. For rocks with very poor mechanical properties, as the Palagonia sandstone, the minimum embedment length exceeds ten times the diameter.

From the graphs it is clear that the mechanical behaviour of basalt and limestone is very similar while chemical anchors in sandstone exhibit a poor pull-out strength.

5. Theoretical models for the strength prediction

In the present section some theoretical models of failure mechanisms for chemical anchors in the literature are examined. Specifically, these studies concern the calculation of the chemical anchor tensile load for different failure patterns. The described models are all referred to concrete. However, they were applied to the studied stones, for testing the possibility of their applications also in the case of natural rocks instead of concrete. Material data in Section 3 were used.

5.1. Modelling of chemical anchors in concrete

The modelling of chemical anchors is based on the transfer of the applied load from the steel anchored element, through the adhesive layer, to the concrete along the entire bonded surface.

The literature contains several approaches for the calculation of the failure load in traction of individual chemical anchors as a function of the depth of the anchor. These design approaches have been developed for specific products and they are based on tests changing the different parameters of the problem. Cook and Konz [3] conducted a comprehensive investigation of more than 1000 tests with twenty types of adhesive products. According to this study, the parameters that affect the resistance of a chemical anchor are: adhesive strength; compressive strength of concrete; hole cleaning; humidity of the hole; high temperatures and creep; charging time. Fig. 9 shows the possible failure mechanisms.

1. If the embedment depth is very small, a concrete cone failure occurs.
2. If the depth of the anchor is greater we can have:
   (a) Combined mechanism, given by a shallow concrete cone failure with sliding at the adhesive/concrete interface below the cone.
   (b) Combined mechanism, given by a shallow concrete cone failure with sliding at the rod/adhesive interface below the cone.
   (c) Combined mechanism, given by a concrete cone failure with sliding at the adhesive/concrete interface in the upper part of the anchor and sliding at the rod/adhesive interface in the lower part.
3. If the embedment depth is very high, the anchor is so resistant that the failure occurs for breakage of the steel bar.

In [7] the influence on the failure modes of the proximity of the anchor to the support edge and of the spacing in group anchors is investigated.

The minimum depth for obtaining the rupture of the bar represents the embedment length of the anchor, also depending on the quality of the steel and on the properties of the resin. Table 5 summarizes the main models used to predict the strength of the bonded anchors.

Model 1 is an *elastic bond-stress model* [28]; the model addresses compatibility relationships between concrete, bonding agent and threaded rod.

Model 2 is a *uniform bond-stress model* [10] and it predicts the capacity of the anchor as a function of the uniform failure stress τ_0.

Model 3 is a *uniform bond-stress model with real resistance of adhesive* [1]; the bond area effect can be represented by an additional modification factor (ψ_b).

Model 4 is a *bond models neglecting the shallow concrete cone* [5], where the effective embedment length is equal to the actual embedment length minus 3 times the diameter, to account for the shallow concrete cone.

Models 5 and 6 [5,2] are *combined cone-bond models*: model 5 is *combined concrete cone/ bond model uniform*; model 6 is *combined concrete cone/bond model elastic*.

Models 7 and 8 [29] are *interface bond model*: model 7 is based on the sliding at the *adhesive/concrete interface*; model 8 is based on the sliding at the *steel/adhesive interface*.

Model 9 is a *concrete cone model* [30].

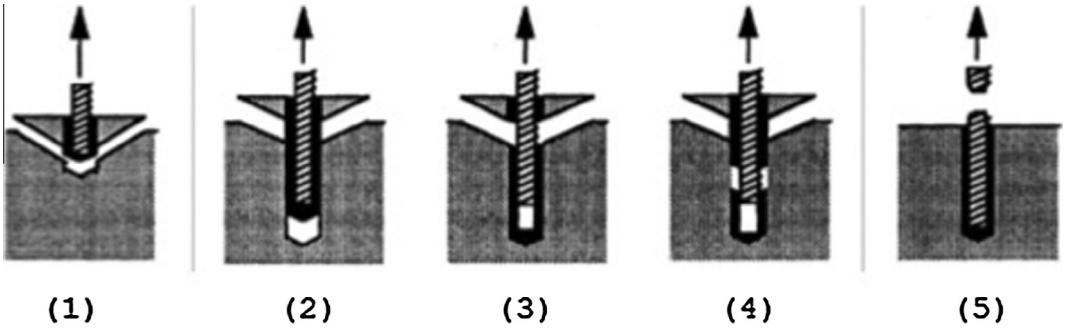

Fig. 9. Breaking mechanisms.

Table 5
Theoretical concrete models for the prediction of the ultimate anchor strength.

Model	Author	Ultimate axial force
1	Doerr et al. [28]	$N_u = \tau_{max}\pi d_0\left(\frac{d_0}{\lambda'}\tanh\frac{\lambda' h_{ef}}{\sqrt{d_0}}\right)$
2	McVay et al. [10]	$N_u = \tau_0\pi d_0 h_{ef}$
3	Nilson [1]	$N_u = \tau_0\pi d_0\Psi_b\Psi_c$
4	Cook et al. [6]	$N_u = \tau\pi d(h_{ef} - 3d)$
5	Cook et al. [5]	$N_u = 0.92h_{ef}^2\sqrt{f'} + \tau_0\pi d_0 h_{ef}$
6	Cook [2]	$N_u = 0.92h_{ef}^2\sqrt{f'} + \tau_{max}\pi d_0\left(\frac{d_0}{\lambda'}\tanh\frac{\lambda' h_{ef}}{\sqrt{d_0}}\right)$
7	Marti [29]	$N_u = \tau\pi d h_{ef}$
8	Marti [29]	$N_u = \tau\pi d h_{ef}\sqrt{\frac{f_c}{f_{c,bw}}}$
9	Eligehausen et al. [30]	$N_u = 0.92\ h_{ef}^2\sqrt{f'}$

The results obtained by using the theoretical models above are collected in Tables 6–8. The calculations have been carried out considering the mechanical properties of the materials under investigation.

Data show the predictions for fixed stone type, by varying the rod diameter and the embedment length. In the columns labeled N_u all the predicted values exceeding the theoretical yield force (equal to 35.3 kN, 69.3 kN and 141.4 kN for steel rods with nominal diameter equal to 10 mm, 14 mm and 20 mm, respectively) are meaningless, because the yielding precedes the mechanism.

5.2. Theoretical prediction vs experimental results

Figures from 10–13 show the comparison between the pull-out strength predictions given by using formulas in Table 5 and the

Table 6
Predictions of theoretical models for Palagonia sandstone anchor.

	Palagonia sandstone								
	ϕ10			ϕ14			ϕ20		
	3ϕ N_u (kN)	5ϕ N_u (kN)	10ϕ N_u (kN)	3ϕ N_u (kN)	5ϕ N_u (kN)	10ϕ N_u (kN)	3ϕ N_u (kN)	5ϕ N_u (kN)	10ϕ N_u (kN)
Model 1	0.5	0.5	0.5	0.8	0.8	0.8	1.3	1.3	1.3
Model 2	5.7	9.5	19.0	10.3	17.1	34.2	19.5	32.6	65.1
Model 3	6.3	10.2	19.5	10.9	17.6	33.8	19.9	32.1	61.6
Model 4	0.0	3.0	10.6	0.0	5.9	20.7	0.0	12.1	42.2
Model 5	3.5	7.3	16.8	6.6	13.5	30.6	13.1	26.1	58.7
Model 6	4.2	10.8	41.7	8.1	21.0	81.5	16.1	42.4	165.9
Model 7	4.5	7.5	15.1	8.9	14.8	29.6	18.1	30.2	60.3
Model 8	5.7	9.5	19.0	10.3	17.1	34.2	19.5	32.6	65.1
Model 9	3.7	10.3	41.1	7.3	20.2	80.6	14.8	41.1	164.6
Experimental	4.6	14.2	17.0	9.3	15.2	26.0	11.7	30.7	73.0

Table 7
Predictions of theoretical models for Etna basalt anchor.

	Etna basalt								
	ϕ10			ϕ14			ϕ20		
	3ϕ N_u (kN)	5ϕ N_u (kN)	10ϕ N_u (kN)	3ϕ N_u (kN)	5ϕ N_u (kN)	10ϕ N_u (kN)	3ϕ N_u (kN)	5ϕ N_u (kN)	10ϕ N_u (kN)
Model 1	5.6	5.6	5.6	8.5	8.5	8.5	13.6	13.6	13.6
Model 2	59.4	99.0	197.9	106.9	178.1	356.3	203.6	339.3	678.6
Model 3	65.6	106.1	203.5	113.4	183.3	351.8	207.0	334.6	641.9
Model 4	0.0	31.4	110.0	0.0	61.6	215.5	0.0	125.7	439.8
Model 5	11.8	51.4	150.3	28.2	99.4	277.6	63.7	199.4	538.7
Model 6	24.1	57.0	211.3	44.8	109.3	411.7	87.7	219.3	836.5
Model 7	47.1	78.5	157.1	92.4	153.9	307.9	188.5	314.2	628.3
Model 8	59.4	99.0	197.9	106.9	178.1	356.3	203.6	339.3	678.6
Model 9	18.5	51.4	205.7	36.6	100.8	403.2	74.1	205.7	822.9
Experimental	25.2	34.1	33.6	46.1	68.6	72.2	90.6	141.2	142.8

Table 8
Predictions of theoretical models for Floresta limestone anchor.

	Floresta limestone								
	ϕ10			ϕ14			ϕ20		
	3ϕ N_u (kN)	5ϕ N_u (kN)	10ϕ N_u (kN)	3ϕ N_u (kN)	5ϕ N_u (kN)	10ϕ N_u (kN)	3ϕ N_u (kN)	5ϕ N_u (kN)	10ϕ N_u (kN)
Model 1	2.6	2.6	2.6	3.9	3.9	3.9	6.3	6.3	6.3
Model 2	26.4	44.0	88.0	47.5	79.2	158.3	90.5	150.8	301.6
Model 3	29.2	47.1	90.4	50.4	81.5	156.3	92.0	148.7	285.3
Model 4	0.0	14.5	50.6	0.0	28.3	99.1	0.0	57.8	202.3
Model 5	12.5	30.1	74.1	24.6	56.2	135.4	49.7	110.1	260.8
Model 6	15.1	37.5	142.1	28.5	72.3	277.4	56.5	145.8	564.4
Model 7	21.7	36.1	72.3	42.5	70.8	141.6	86.7	144.5	289.0
Model 8	26.4	44.0	88.0	47.5	79.2	158.3	90.5	150.8	301.6
Model 9	12.6	34.9	139.5	24.6	68.4	273.5	50.2	139.5	558.1
Experimental	22.3	34.4	33.8	38.6	40.1	58.0	60.4	101.0	141.0

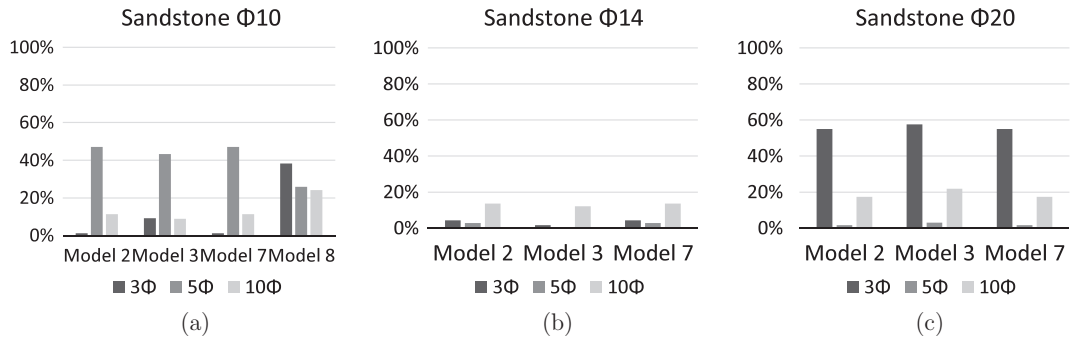

Fig. 10. Sandstone. Percentage error of the theoretical predictions w.r.t. experimental results. (a) $\phi = 10$ [mm]. (b) $\phi = 14$ [mm]. (c) $\phi = 20$ [mm].

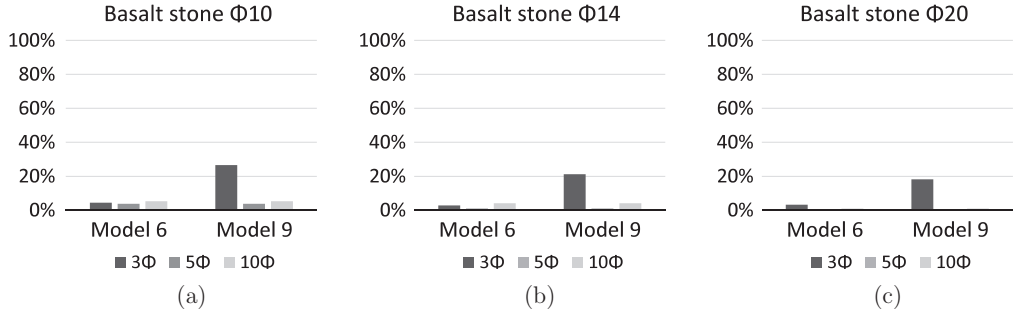

Fig. 11. Basalt stone. Percentage error of the theoretical predictions w.r.t. experimental results. (a) $\phi = 10$ [mm]. (b) $\phi = 14$ [mm]. (c) $\phi = 20$ [mm].

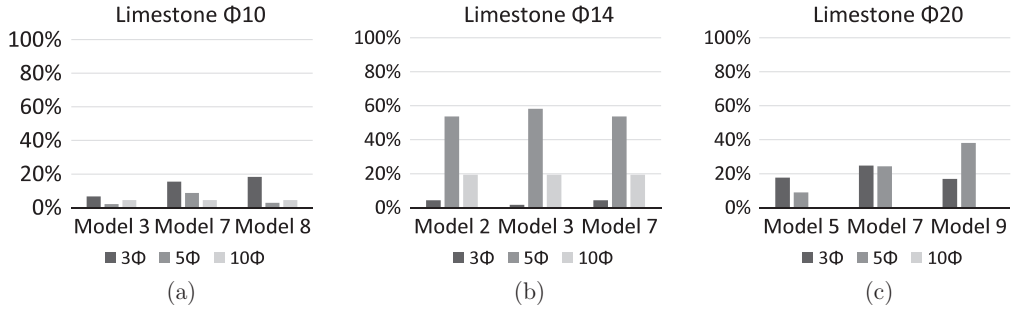

Fig. 12. Limestone. Percentage error of the theoretical predictions w.r.t. experimental results. (a) $\phi = 10$ [mm]. (b) $\phi = 14$ [mm]. (c) $\phi = 20$ [mm].

experimental results in Section 4.3. According to the rupture mechanism exhibited in the series, only the compatible theoretical models have been applied. The minim value between the Model *n* prediction of the pull-out force N_u and the theoretical yield force in the steel bar is considered.

In the case of Etna basalt, the prediction given by model 6 provides excellent results, with error in the range 0.12–5.22%, as it is shown in Fig. 11.

Regarding limestone, Fig. 12 shows that model 7 provides the more reliable prediction of the pull-out forces for the three tested anchoring lengths. The prediction for diameters $\phi = 10$ [mm] and $\phi = 20$ [mm] (Fig. 12(a and c)) are more accurate compared to the predictions for the diameter $\phi = 14$ [mm] (Fig. 12(b)).

In Fig. 10 the results for sandstone are reported. Predictions concerning sandstone appeared feasible by using models 2, 3 and 7. However, in this case the results are less accurate compared to the previous cases.

The analysis of the comparisons highlights that concrete models present in the literature for the prediction of the ultimate strength of anchoring systems with resin can be applied to natural stones if the mechanical characteristics of the stone are quite similar to the ones of a normal concrete for construction, with values of the rupture stress in compression between 20.0 and 50.0 [MPa].

The aforementioned consideration are again confirmed by the bar charts in Fig. 13(a–c), that show the comparison of the percentage error in the predictions for fixed embedment length, by varying the stone type.

6. Numerical analysis

In this section, the possibility of providing a numerical prediction of the capacity of the anchor is investigated. Numerical models were built with the commercial software Adina (version 8.8).

6.1. Constitutive models

Thanks to the polar symmetry of the geometrical and mechanical characteristics of the problem, the numerical simulations were carried out under the axisymmetric stress regime. Therefore, just a

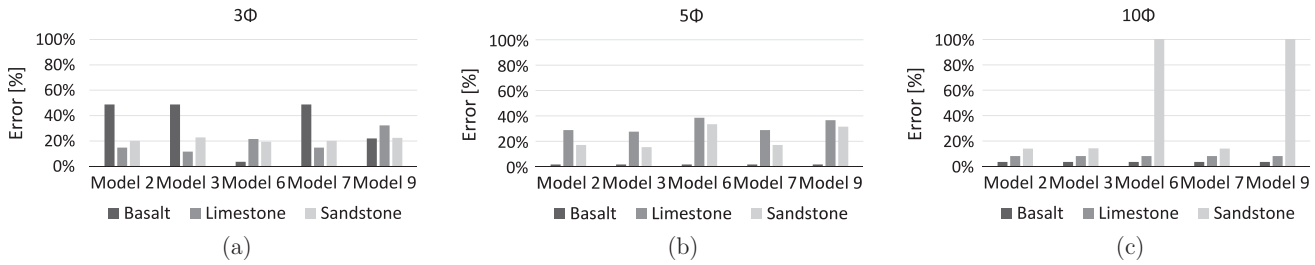

Fig. 13. Percentage error of the pull-out strength theoretical predictions w.r.t. experimental results for different embedment depth. (a) $L = 3 \cdot \phi$. (b) $L = 5 \cdot \phi$. (c) $L = 10 \cdot \phi$.

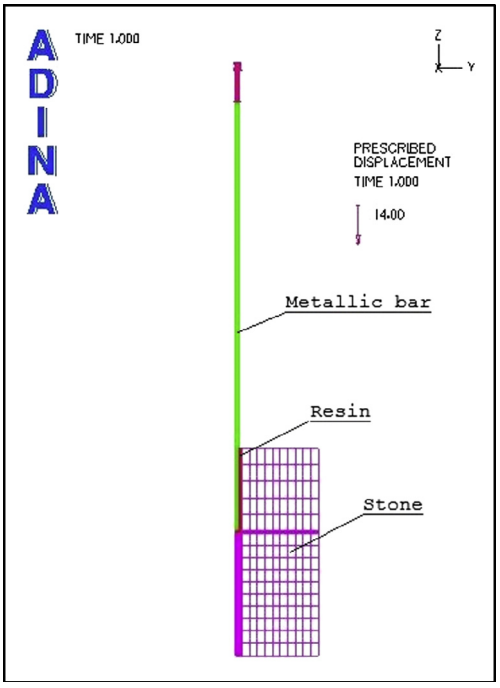

Fig. 14. FEM axis-symmetric model.

1 radian central angle portion of the system was discretised, as it is shown in Fig. 14. Therefore, roller supports allowing vertical displacements were entered along the bar axis and roller supports allowing horizontal displacements were entered along the base of the model.

The loading condition consisted in the self weight and in imposed vertical displacement at the top end of the steel bar.

The steel bar was modelled according to a standard bilinear constitutive law with hardening.

The resin was hypothesised as linearly elastic. Indeed, in the strain range involved in the crisis mechanisms, representative of short-term static loadings at ambient temperatures, the assumption can be considered as realistic, as it can be deduced by the experimental results concerning the behaviour of an epoxy resin under multiaxial stress states reported in [31] and from the characterisation of the long-term performance of epoxy-bonded anchor system in concrete presented in [32]. However, resins used in structural applications can exhibit significant viscoelastic response to long-term loadings, especially at elevated temperatures [14]. Therefore, in the study of creep phenomena involving adhesively bonded anchors viscosity must be incorporated in the modelling.

Three different constitutive models were tested for what concern the stone: the *Mohr–Coulomb model*, the *Drucker–Prager model*, *the Concrete model* [33]. The mechanical parameters entering the model of the rocks, that is the friction angle and the cohesion, were evaluated in terms of the tensile and compressive strength of the materials given in Section 3.

6.2. Numerical predictions vs experimental results

All the eighty-one experimental tests in section 4.3 were numerically reproduced.

For same series of experimental tests there was a significant difference among the results concerning the samples of the series itself, the differences being related to the failure mechanism. For this reason, when the case occurred, the comparison was made between the numerical results and the experimental data correlated to a single test, for which the failure behaviour was well defined, and not the mean value.

The analyses always provided a reliable value of the ultimate strength. Only in the case of test B-10-3 the result was not admissible, where the effective crisis was in the stone, while a rod failure was predicted by the numerical simulation. However, a stiffer behaviour of the model affects the simulations of pull-out tests with the lower embedment length $L = 3 \cdot \phi$, as it can be seen for instance in pictures Fig. 15(a and b) in the case a Mohr–Coulomb criterion is adopted for the stone material. A similar behaviour can be recovered by a Drucker–Prager model. By using the Microplane Concrete Model the convergence was often lost well before the peak load.

It has been observed that the pathologic behaviour of the model, when considering a short embedment length, can be ascribed to the hypothesis of axis-symmetric regime. In that case it has been verified that the same inaccuracy characterises plain strain simulations, while an additional analysis carried out in plane stress, using for simplicity the Von Mises constitutive model under the hypothesis of elastic–plastic behaviour without hardening, showed the right prediction of the stiffness (see Fig. 16). That is, in the case of very short embedment length, a stress state accounting for confinement actions is not adequate in reproducing the physical behaviour, in agreement with what observed in [10].

For basalt and limestone the peak load prediction was accurate for $L = 5 \cdot \phi$ and $L = 10 \cdot \phi$, being the crisis related to the yielding of the steel bar, as it is shown in Fig. 17. For sandstone the crisis stone cone was always correctly predicted, both in term of pull-out strength and stiffness of the system, as it can be observed in Fig. 18. Fig. 19 show the evolution of the Mohr–Coulomb yield function in the case of test A-20-5.

Fig. 20 shows the bar chart of the percentage error in the estimation of the pull-out strength. It has once again to be underlined that the good agreement of the numerical results with the simulations for basalt and limestone with anchor length L equal to $5 \cdot \phi$ and $10 \cdot \phi$ is valid just because the rupture coincides with the yielding of the steel rod, totally ruled by the elastic plastic model of the steel.

From the pictures it is clear that a uniform trend in the numerical prediction cannot be recovered. The reason can be ascribed to mixed failure mechanisms, due to unpredictable physical and

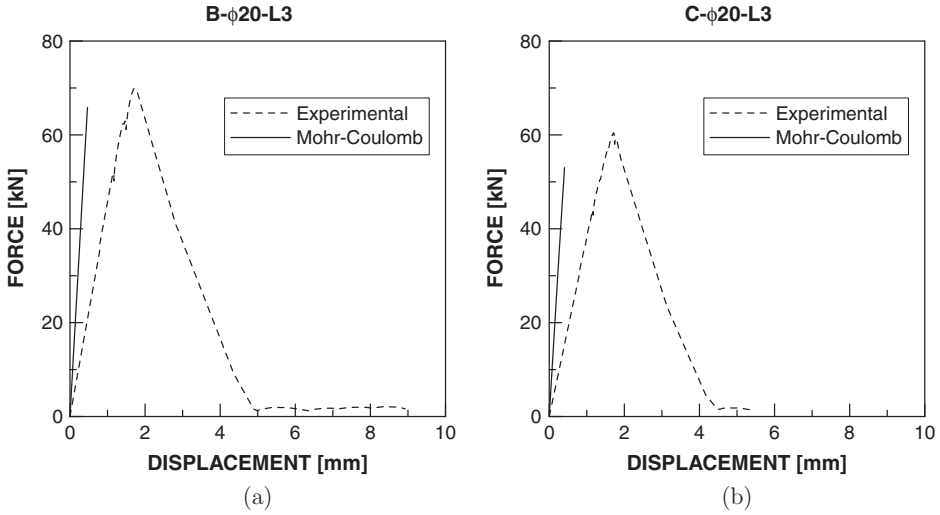

Fig. 15. Mohr–Coulomb prediction. (a) Basalt $\phi = 20$ [mm], $L = 3 \cdot \phi$. (b) Limestone $\phi = 20$ [mm], $L = 3 \cdot \phi$.

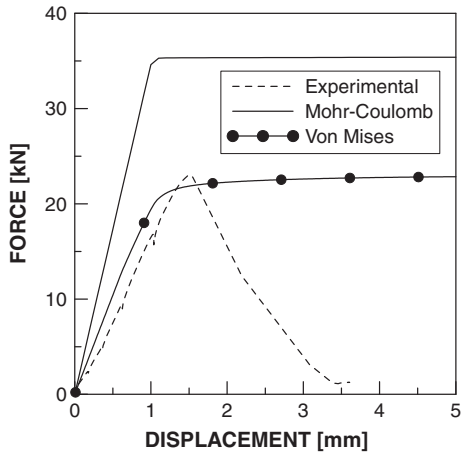

Fig. 16. Von Mises plane stress elastic–plastic simulation of test B-10-3 compared with plane strain Mohr Coulomb model.

mechanical phenomena arising during the physical cracking process and also caused by imperfect bonding, whose prediction by means of numerical simulation is not feasible. Despite the inaccurate determination of the limit strength, the limit value of the embedment depth, separating the rock failure from the steel failure is correctly identified.

On the contrary, when the crisis mechanism is well known and the materials properties correctly identified, appropriate numerical simulations can reproduce a posteriori the phenomenon with high accuracy and precision, provided that adequate modelling are used. In the following section a specific algorithm for the prediction of the cracks in brittle material is applied as an explanatory example, but not exclusive.

7. Comparison of the experimental results with a Finite Element with Embedded Discontinuity simulation

Failure of concrete-like materials or rocks is characterised by the growth and propagation of cracks that can arise in unpredictable location of the body.

Theoretical and numerical procedures can be used to predict the stress distribution during the pre-critic phase and the peak load. Usually this predictions are made under the hypothesis of linearly elastic materials or in the field of Linear Fracture Mechanics.

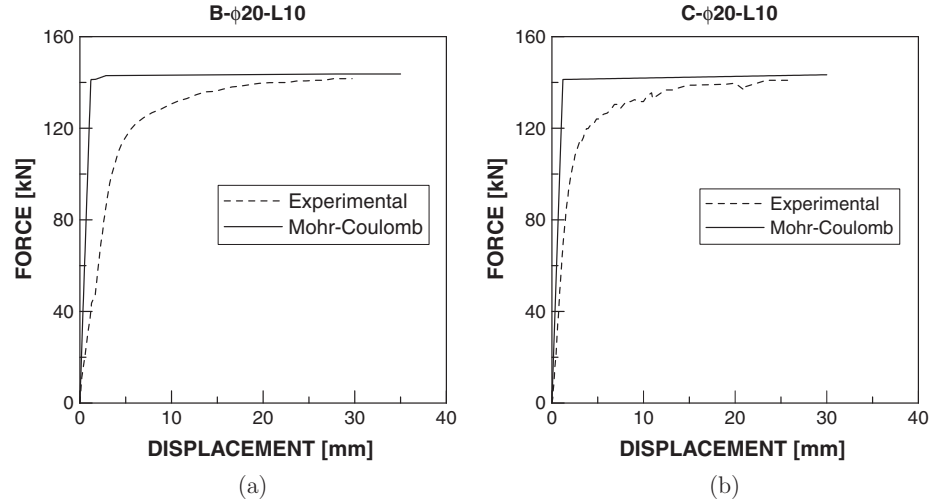

Fig. 17. Steel rod failure prediction. (a) Basalt ϕ=20 [mm], $L = 10 \cdot \phi$. (b) Limestone $\phi = 20$ [mm], $L = 10 \cdot \phi$.

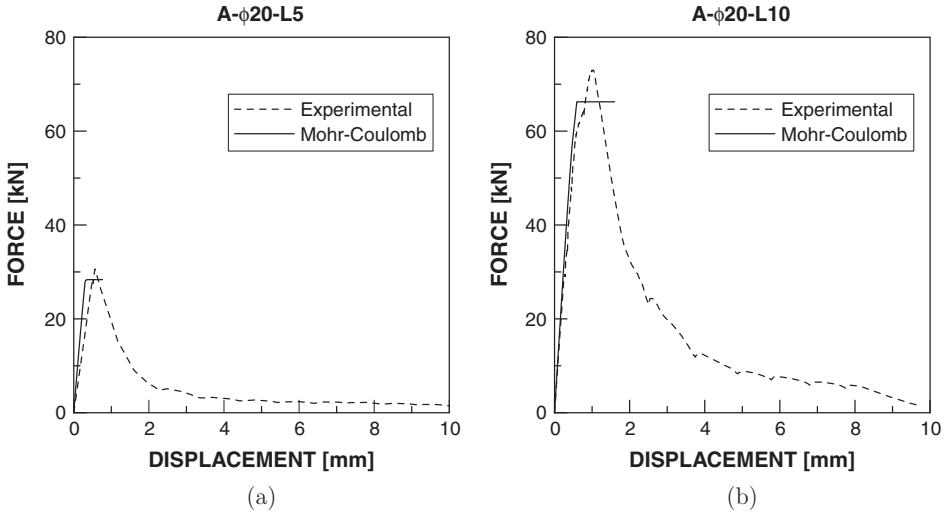

Fig. 18. Sandstone failure prediction (a) $\phi = 20$ [mm], $L = 5 \cdot \phi$. (b) $\phi = 20$ [mm], $L = 10 \cdot \phi$.

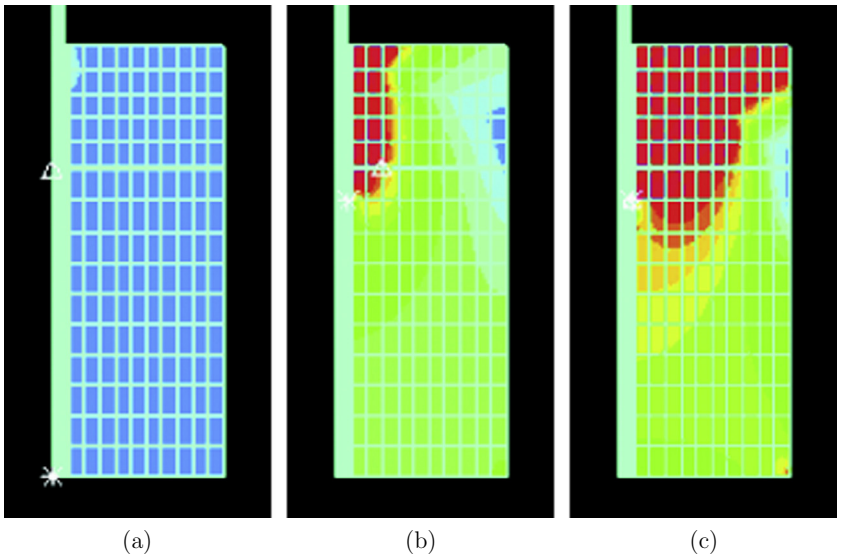

Fig. 19. Failure evolution for sandstone $\phi = 20$ [mm], $L = 5 \cdot \phi$ sample. Mohr Coulomb yield function.

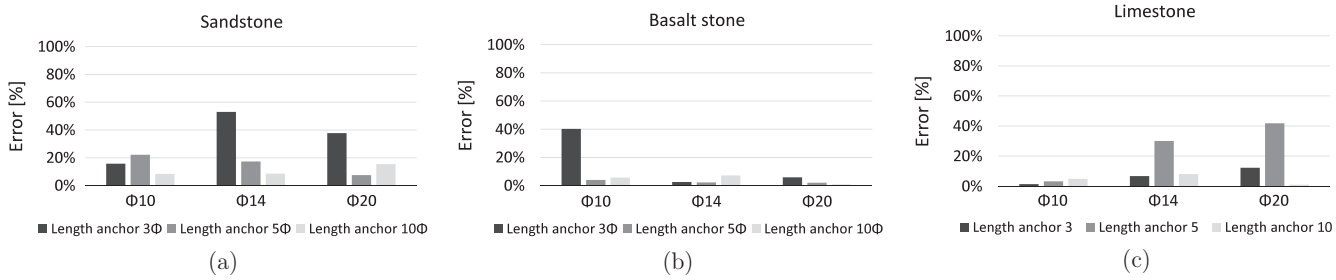

Fig. 20. Percentage error of the numerical pull-out strength predictions w.r.t. experimental results for different stone type. (a) Sandstone. (b) Basalt. (c) Limestone.

However, the study of the post-critic behaviour necessitates the introduction in the theoretical models of more sophisticated characteristics both for the constitutive laws and the kinematics.

For instance, constitutive models accounting of the different behaviour of these materials under compressive, tensile or confined stress states can be used in the analysis, in the way shown in Section 6, where Mohr–Coulomb and Drucker–Prager criterion have been introduced for modelling the irreversible behaviour of the stone material. In term of enrichment of the kinematics many approaches exist in the literature and are successfully exploited.

A number of formulations is based on the Strong Discontinuity Approach (SDA), starting from the pioneer works by [34,35], the differences originating from the numerical implementation in the Finite Element Method. Elements with Embedded Discontinuities [36–38] and the eXtended Finite Element Method [39–41] are the main tools for the discrete description of the problem.

In all this models the crack opening is ruled by specific interface activation functions playing the role of the yield function in plasticity. The method has successfully been adopted in the prediction of crack growth and propagation in concrete-like materials, reinforced concrete structural members, etcetera.

In this section the numerical model based on the Strong Discontinuity Approach (SDA) and proposed in [42,43] has been applied to the analysis of the post-installed adhesive anchors under investigation. Cracks are numerically simulated by a jump in the displacement field, that can be physically identified with the discontinuity surface that arises, for instance, in the failure mechanism previously described with development of a cone in the rock. The opening of cracks, assimilated to the growth of interfaces, is ruled by a cohesive fracture activation function. The numerical algorithm falls in the context of the Finite Elements with Embedded Discontinuity. It was implemented in the FracSDA8 code developed in [44].

As an example, the simulation of test B-10-3 was performed, under the hypothesis of plane stress. In fact, in the test in question the embedment depth is equal to 3 times the diameter, i.e. 3 [cm]. Therefore, the anchoring is so near the surface of the stone block that the confinement characterising axis-symmetric stress states is negligible and the plane stress state hypothesis is admissible.

The prediction of the numerical application largely agrees with the experimental result, both in terms of failure mechanism and in term of ultimate strength of the anchor. The picture in Fig. 21(a) shows the vector plot of the principal stresses, in which the direction of the minimum principal stress gives the trend of the fracture, this direction being normal to the maximum tensile principal stress. The peak load corresponding to the initial crack given by

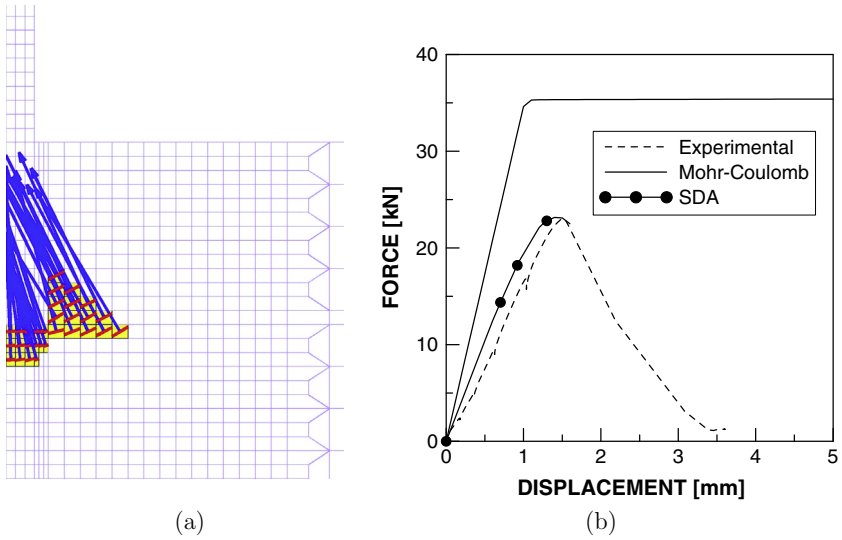

Fig. 21. Test B-10-3. SDA simulation. (a) Vector plot of the principal stress. (b) Force–displacement curve.

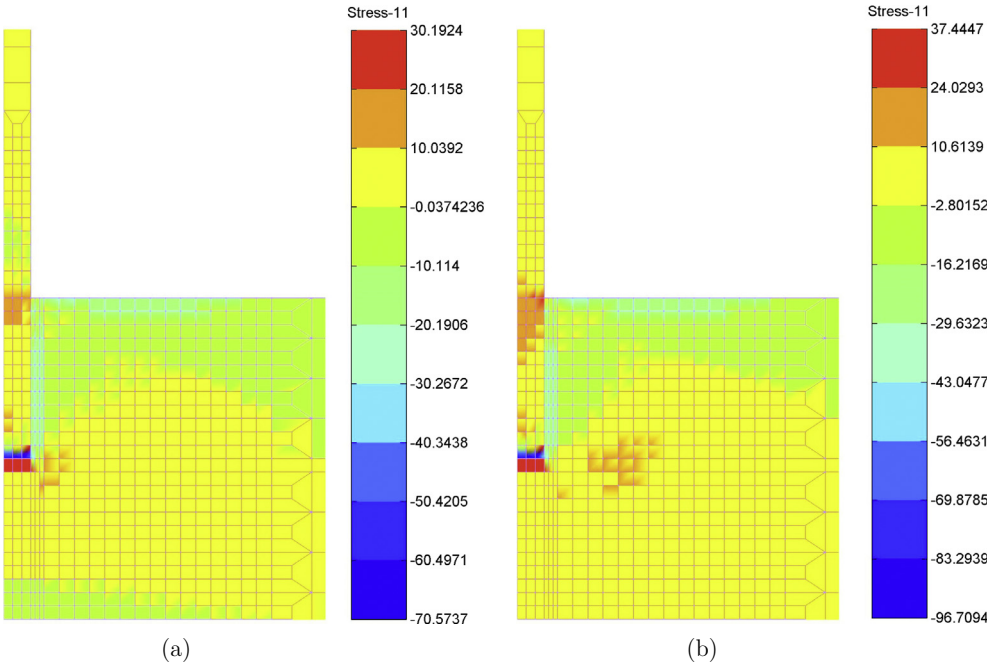

Fig. 22. Test B-10-3. Evolution of the failure mechanism. Tensile principal stress. (a) Activation at the bottom end of the bar. (b) Development of the shear band.

the numerical analysis is in good agreement with the experimental one, as it is shown in Fig. 21(b).

The model is able to accurately predict the initial activation of the failure, that starts for detachment of the bottom end of the bar, under a preponderant tensile stress state in that area. Then, failure progresses and develops along a shear band, with angle equal about to the friction angle of the stone, as it can be seen in Fig. 22.

In the light of the results shown in this section, if compared with the predictions given by the simulations in Section 6, it can be confirmed that the numerical prediction of the entire phenomenon, that is actually complex due to the presence of three different material characterised by quite different mechanical properties and constitutive behaviour, requires more sophisticated computational tools for capturing all the evolution of the crisis process, as for instance the one used in the present section or many other, equally rich, often implemented in advanced commercial F.E. codes.

8. Conclusions

Despite the specific legislation on the architectural heritage prohibits anchoring systems bonded by means of resin on historical and monumental building, but suggest the usage of special mortars, there is a wide range of situations in which the use of chemical anchoring in block masonry is more suitable than mortar. Moreover, the method can be applied every time the masonry buildings are not under a preservation order or listed buildings.

The anchoring systems in natural stone supports based on chemical bond lack extensive studies and laboratory tests. The study and the experiments conducted at the Laboratory of Structural and Material Testing of Catania University during this work have led to the definition of a standard for the installation of such post-installed chemically bonded anchors in specific natural stones. Specifically three types of rock typical of eastern Sicily have been considered, with decreasing mechanical properties. The parameter governing the efficiency of the anchor has been identified in the minimum embedment depth, defined as a function of the rod diameter. This was defined as the minimum value of the embedded length of the steel bar such that the failure occurs in the form of yielding of the bar. The influence of the type of rock on the minimum embedment depth have been classified as a function of the compressive strength of the material. Depending on the embedment length and on the bar diameter, different failure mechanisms have been observed, mainly characterised, for embedment lower than the minimum required, by the development of a cone of rupture of given angle, strictly related to the friction angle of the rock material. In sporadic cases a combined mechanism of cone with sliding at the interface between the rod and the resin appeared. Such cases can be ascribed to a bad adhesion between the rod and the resin, possibly due to the effect of the threading during the insertion of the rod inside the hole, despite the installation procedure was properly carried out.

It was observed that in the case of high performing stone, i.e. basalt and limestone, the resistance of the anchorage is higher, the geometry being equal, if compared to concrete anchor. The opposite result was obviously found in the case of sandstone anchor.

The tested embedment depth were equal to 3, 5 and 10 times the bar diameter. On the basis of the experimental results, the following conclusion was achieved: the minimum anchor length is greater than 3 times the diameter but smaller than 5 times the diameter in the case of basalt and limestone. On the contrary, in the case of the sandstone, the anchor length is greater than 10 times the diameter, because the failure always occurred in the way of cone or cone combined with rock-rock sliding at the bottom part of the bar. The last foreseeable results can be ascribed to the really poor characteristics of this type of rock. These values can safely be applied for chemical anchor in block masonry, because they were determined in absence of confinement pressure, whose presence in in situ conditions increase the pull-out strength of the system. However, it must be highlighted that the aforementioned recommendation concerning the embedment depth is affected by many factors [3]. Among them, beyond the rock compressive strength, the steel grade, the rod diameter and the bar characteristics (headed bolt, threaded rod, steel reinforcing bar). A change in one of this parameters can indeed introduce a variation in the failure mode, from steel breakout to splice failure or combined failure by pullout of a partial-depth stone spall and bond failure in the lower portion of the hole. Moreover, the load capacity of the epoxy resin is significantly affected by the hole size. Therefore the recommendation should be handle with care. For this reason the embedment depth suggested by the resin manufacturer are often oversized. For instance, for the resin in question, the suggested value for bar diameter in the range $10 \div 14$ [mm] is 11ϕ, while for bar diameter from 20 [mm] on the suggested value is 10.5ϕ. A factor of safety obviously affect those values.

The applicability of a number of literature theoretical models, valid for concrete, extensively treated and experimentally verified for that material, was checked in the present case. These models give the pull-out capacity, in term of limit uniaxial load of the anchor. It was found out that, because all the theoretical formulas substantially depends on the strength and stiffness properties of the anchoring system and especially of the support material, that is concrete in their original statement, as well as on purely geometrical quantities, every time the stone properties are close to the concrete ones the predictions are absolutely reliable. On the contrary, this assertion fails in the case of materials with quite different mechanical properties with respect to concrete.

Numerical predictions assuming, in turn, three different constitutive models for the rocks, i.e. a Mohr–Coulomb criterion, a Drucker–Prager criterion and the Microplane Concrete Model, and always considering an elastic–plastic behaviour with hardening for the steel bar and an elastic behaviour for the resin, were performed. The results are in agreement with the experimental evidence in term of ultimate strength only in the case of larger embedment depth, when the rupture happens in the rod, that is only for basalt and limestone. In that situations the elastic–plastic behaviour of the steel rod rules the problem. Moreover, when the material properties are very poor, so that large embedment is needed, the predictions are inaccurate and not reliable. The reason can be ascribed to the effective mixed failure mechanisms arising in this case, due to unpredictable physical and mechanical phenomena, also caused by possible imperfect bonding, whose prediction by means of numerical simulation is not feasible. In the author's opinion, numerical simulations can be adopted as a predictive instrument mainly in the philosophy of finding the minimum embedment length to obtain steel rod failure. This approach can be easily pursued by technicians and licensed engineers by using standard engineering tools. More sophisticated models, requiring the use of advanced numerical codes, have to be used for reproducing the complete evolution of the cracking process.

Acknowledgements

The authors sincerely are grateful to Mr. Pietro Sciacca, Engineer and Technical Coordinator at the Laboratory of Structural and Material Testing, University of Catania, for his suggestion about the research and technical assistance. Moreover, special

thanks go to Mr. N. Salanitri and Ms. A. Burruto for their participation in the experimental tests.

References

[1] Nilson AH. Internal measurement of bond slip. ACI J 1972;69(7):439–41.
[2] Cook RA. Behavior of chemically bonded anchors. J Struct Eng 2001;119(9):2744–62.
[3] Cook RA, Konz RC. Factors influencing bond strength of adhesive anchors. ACI Struct J 2001;98(1):76–86.
[4] Rizzo P, Spada A, Degala S, Giambanco G. Acoustic emission monitoring of chemically bonded anchors. J Nondestruct Eval 2010;29:49–61.
[5] Cook RA, Doerr GT, Klingner RE. Bond stress model for design adhesive anchors. ACI Struct J 1993;90(5):514–24.
[6] Cook RA, Kunz J, Fuchs W, Konz RC. Behavior and design of single adhesive anchors under tensile load in uncracked concrete. ACI Struct J 1998;95(1):9–26.
[7] Eligehausen R, Cook RA, Appl J. Behavior and design of adhesive bonded anchors. ACI Struct J 2006;103(6):822–31.
[8] Çolak A. Estimation of ultimate tension load of methylmethacrylate bonded steel rods into concrete. Int J Adhes Adhes 2007;27:653–60.
[9] Bickel TS, Fattah Shaikh A. Shear strength of adhesive anchors. PCI J 2002:92–102. September–October.
[10] McVay M, Cook R, Krishnamurthy K. Pullout simulation of postinstalled chemically bonded anchors. J Struct Eng 1996;122(9):1016–24.
[11] Ožbolt J, Eligehausen R, PeriŠkić G, Mayer U. 3D FE analysis of anchor bolts with large embedment depths. Eng Fract Mech 2007;74:168–78.
[12] Prieto-Muñoz PA, Yin HM, Testa RB. An elastic analysis that predicts the pull-out capacity of adhesive anchors. In: Proceeding of WCCM/APCOM 2010, vol. 10 of IOP conf. series: materials science and engineering. IOP Publishing; 2010. p. 1–22.
[13] García J, Chiminelli A, García B, Lizaranzu M, Jiménez M. Characterization and material model definition of toughened adhesives for finite element analysis. Int J Adhes Adhes 2011;31:182–92.
[14] James RW, De la Guardia C, McCreary CR. Strength of epoxy-grouted anchor bolts in concrete. J Struct Eng 1987;113(12):2365–81.
[15] Zhao Y, Yang M. Pull-out behavior of an imperfectly bonded anchor system. Int J Rock Mech Min Sci 2011;48(3):469–75.
[16] Sakla SSS, Ashour AF. Prediction of tensile capacity of single adhesive using neural networks. Comput Struct 2005;83:1792–803.
[17] Benmokrane B, Zhang B, Chennouf A. Tensile properties and pullout behaviour of AFRP and CFRP rods for grouted anchor applications. Constr Build Mater 2000;14:157–70.
[18] Kim SJ, Smith ST. Pullout strength models for FRP anchors in uncracked concrete. J Compos Constr 2010;14(4):406–14.
[19] Çolak A. Parametric study of factors affecting the pull-out strength of steel rods bonded into precast concrete panels. Int J Adhes Adhes 2001;21:487–93.
[20] Yilmaz S, Ozen MA, Yardim Y. Tensile behavior of post-installed chemical anchors embedded to low strength concrete. Constr Build Mater 2013;47:861–6.
[21] Çallşkan O, Yllmaz S, Kaplan H, Klraç N. Shear strength of epoxy anchors embedded into low strength concrete. Constr Build Mater 2013;38:723–30.
[22] Barnat J, Bajer M, Vyhnánková M. Bond strength of chemical anchor in high-strength concrete. In: Steel structures and bridges, vol. 40 of procedia engineering; 2012. p. 38–43.
[23] Cimadevila JE, Chans DO, Gutiérrez EM, Rodríguez JV. New anchoring system with adhesive bulbs for steel rod joints in wood. Constr Build Mater 2012;30:583–9.
[24] Cimadevila JE, Chans DO, Gutiérrez EM. Adhesive multi-bulbs: a novel anchoring system using threaded steel rods glued into wood. Constr Build Mater 2013;48:131–6.
[25] Lombillo I, Thomas C, Villegas L, Polanco JA, Setin J, Biezma MV. Mechanical behavior of anchorages for reinforcing marine stone structures subjected to sea waves. Int J Adhes Adhes 2011;23(5):682–91.
[26] Algin HM. Investigation of masonry wall fixings subject to pullout load and torque. Constr Build Mater 2007;21:2041–6.
[27] Kılłlc A, Yasar E, Celik A. Effect of grout properties on the pull-out load capacity of fully grouted rock bolt. Tunn Undergr Sp Technol 2002;17:355–62.
[28] Doerr GT, Cook RA, Klingner RE. Adhesive anchors: behaviour and spacing requirements. Research report 1126-2. University of Texas, Austin; 1989.
[29] Marti P. Anchoring of concrete reinforcement using HIT-HY 150. Tech. rep.; Hilti Development Corporation; 1993.
[30] Eligehausen R, Mallee R, Rehm G. Befestigungen mit verbundankern (fastenings with bonded anchors). Betomverk + FertigteilTechnik 1984;10:686–92.
[31] Liang YM, Liechti KM. On the large deformation and localization behavior of an epoxy resin under multiaxial stress states. Int J Solids Struct 1996;33(10):1479–500.
[32] Yang M, Zhao Y, Zhang N. Creep behavior of epoxy-bonded anchor system. Int J Rock Mech Min Sci 2014;67:96–103.
[33] Bažant ZP, Prat PC. Microplane model for brittle–plastic material. I: Theory. II: Verification. J Eng Mech 1988;114(10):1672–99.
[34] Simo J, Oliver J, Armero F. An analysis of strong discontinuities induced by strain softening in rate independent inelastic solids. Comput Mech 1993;12:277–96.
[35] Oliver J, Cervera M, Manzoli O. Strong discontinuities and continuum plasticity models: the strong discontinuity approach. Int J Plasticity 1999;15:319–51.
[36] Jirásek M. Comparative study on finite elements with embedded discontinuities. Comput Meth App Mech Eng 2000;188:307–30.
[37] Alfaiate J, Simone A, Sluys L. Non-homogeneous displacement jumps in strong embedded discontinuities. Int J Solids Struct 2003;40:5799–817.
[38] Mosler J. A novel algorithmic framework for the numerical implementation of locally embedded strong discontinuities. Comput Meth App Mech Eng 2005;194:4731–57.
[39] Moës N, Dolbow I, Belytschko T. A finite element method for crack growth without remeshing. Int J Numer Methods Eng 1999;46:131–50.
[40] Belytschko T, Moës N, Usui S, Parimi C. Arbitrary discontinuities in finite elements. Int J Numer Methods Eng 2001;50:993–1013.
[41] Rabczuk T, Zi G. A meshfree method based on the local partition of unity for cohesive cracks. Comput Mech 2007;39(6):743–60.
[42] Contrafatto L, Cuomo M, Fazio F. An enriched finite element for crack opening and rebar slip in reinforced concrete members. Int J Fract 2012;178(1–2):33–50.
[43] Contrafatto L, Cuomo M, Di Venti G. Finite elements with non homogeneous embedded discontinuities. In: European congress on computational methods in applied sciences and engineering, ECCOMAS 2012. Barcelona, Spain; 2012b, p. 9152–71.
[44] Di Venti GT. Modellazione numerica della nascita e dello sviluppo di interfacce mediante il metodo delle discontinuitá forti intraelemento. Ph.D. thesis; Universitá di Catania, Dipartimento di Ingegneria Civile e Ambientale; 2012.